Advances in Materials
2022; 11(3): 69-76
http://www.sciencepublishinggroup.com/j/am
doi: 10.11648/j.am.20221103.13
ISSN: 2327-2503 (Print); ISSN: 2327-252X (Online)

Effect of Secondary Graphitization Expansion on Micro-shrinkage Porosity of Ductile Iron

Shuying Chen[1, *], Qingchun Li[1], Jiajian Song[2], Ming Sun[2], Haiqing Sun[2], Guowei Chang[1]

[1]School of Materials Science and Engineering, Liaoning University of Technology, Jinzhou, China

[2]Jinzhou Jietong Railway Machinery Manufacturing Co., Ltd, Jinzhou, China

Email address:

jinzhouchenshuying@126.com (Shuying Chen)

[*]Corresponding author

To cite this article:

Shuying Chen, Qingchun Li, Jiajian Song, Ming Sun, Haiqing Sun, Guowei Chang. Effect of Secondary Graphitization Expansion on Micro-shrinkage Porosity of Ductile Iron. *Advances in Materials*. Vol. 11, No. 3, 2022, pp. 69-76. doi: 10.11648/j.am.20221103.13

Received: June 28, 2022; **Accepted**: July 27, 2022; **Published**: August 9, 2022

Abstract: Secondary graphitization annealing is often used to obtain 100% ferrite matrix in the production of ductile iron. The volume expansion of pearlite will occur during secondary graphitization annealing. So far, whether this expansion can affect the micro-shrinkage porosity between the austenite rings surrounding the graphite nodule during solidification has not attracted people's attention, while micro-shrinkage porosity is one of the primary factors affecting the impact toughness of ductile iron at ultra-low temperature. Aiming at the problem of whether the secondary graphitization of ductile iron affects the micro-shrinkage porosity, the secondary graphitization annealing of pearlitic ductile iron is carried out, and the effect of secondary graphitization expansion on micro-shrinkage porosity was studied. The metallographic microstructures and micro-shrinkage porosity are observed by Axiovert200MAT metallographic microscope and MLA250 (FEIQuanta) scanning electron microscope. The maximum length of micro-shrinkage porosity is measured by Nano Measurer 1.2 and the maximum area is measured by Photoshop software. The results show that the volume expansion rates of ductile iron and gray cast iron after secondary graphitization annealing are about 1.2% and 1.4%, respectively. After secondary graphitization annealing, the size and quantity of micro-shrinkage porosity of ductile iron decrease. It indicates that the expansion after secondary graphitization of cast iron will help to repaire micro-shrinkage porosity.

Keywords: Ductile Iron, Gray Cast Iron, Secondary Graphitization, Expansion Rate, Micro-shrinkage Porosity

1. Introduction

With the increasing use of ductile iron in wind power generation, rail transit, nuclear power, large ships and other fields, the requirements for the mechanical properties of ductile iron are higher and higher, especially the requirements for low-temperature impact toughness [1, 2]. Therefore, people have carried out in-depth research on low-temperature and high-toughness ductile iron. Their main work focuses on strengthening the morphology of graphite ball [3-8] and the alloying of nickel and silicon [9-14]. Some people also have carried out research into the effects of inclusion, phosphorus content and heat treatment process in ductile iron [15-18]. In this paper, the effect of micro-shrinkage porosity on the low temperature toughness of ferritic ductile iron was studied by changing the riser neck diameter. It is found that when the spheroidization rate of ferritic ductile iron is greater than 98% and the number of graphite balls is greater than 810/mm^2, the micro-shrinkage porosity becomes the key factor affecting the ultra-low temperature impact toughness of ductile iron. When the length of micro-shrinkage porosity is less than 3.7μm, the impact energy of ferritic ductile iron can still reach more than 12J.cm^{-2} at -70°C [19].

Secondary graphitization annealing is often used to obtain 100% ferrite matrix in the production of ductile iron. The volume expansion of pearlite will occur during secondary graphitization annealing. So far, whether this expansion can affect the micro-shrinkage porosity between the austenite rings surrounding the graphite ball during solidification has not attracted people's attention, let alone the corresponding research results. Therefore, this paper mainly studies the effect of secondary graphitization annealing on micro-shrinkage porosity to provide a theoretical basis for the production of

ferritic ductile iron with high toughness in the ultra-low temperature.

2. Experiment

Using 500kg medium frequency induction furnace to melt the furnace burden that consists of pig iron and scrap steel, and the temperature from furnace of molten iron is 1510°C - 1530°C. The pour-over spheroidizing treatment was carried out by using Fe-46Si-6Mg-1RE alloy as spheroidizing agent. The secondary inoculation treatment was carried out by using Silicon-Barium pregnant agent and the flow inoculation treatment was carried out by using Sulfur-Oxygen pregnant agent. The pouring temperature is 1380°C -1440°C. The chemical composition of the experimental raw materials and ductile iron is shown in Table 1.

Table 1. *Chemical composition of raw materials and cast iron for experiment (wt%).*

	C	Si	Mn	P	S	RE	Mg	Ba	Ti	Ca	Al	O
Pig iron	4.6	0.44	0.026	0.025	0.02				0.03			
Scrap steel	0.2	0.26	0.54	0.04	0.05							
Spheroidizing agent		44-48				0.85-1.15	5.55-6.15			0.8-1.2	≤1.0	
Si-Ba inoculant		72-78						2.0-3.0		1.0-2.0	≤1.5	
S-O inoculant		70-76			≤1.0	1.5-2.0				0.75-1.25	0.75-1.25	≤1.0
Ductile iron	3.8	2.2	0.15	0.025	0.01	0.02	0.04		0.023			
Grey cast iron	3.8	2.2	0.15	0.025	0.01							

The Y-type samples are prepared using the method of sand mold casting and the size of it is shown in Figure 1. The samples for heat treatment are made by cutting the Y-type samples with the size 25mm×40mm×180mm.

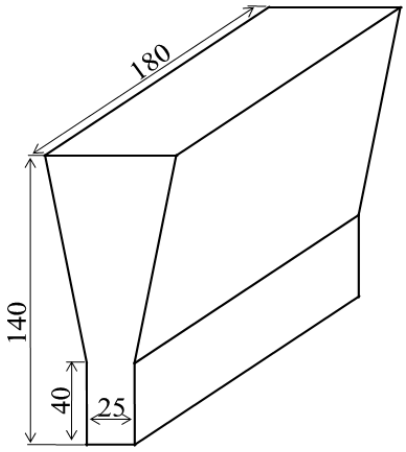

Figure 1. *Schematic diagram of Y-type sample.*

The samples were heated in a box-type resistance furnace and normalized by holding at 880°C and 920°C to adjust the amount of pearlite in the microstructure.

In order to avoid the influence of surface oxidation on the size of the sample, the secondary graphitization annealing of samples is carried out in a vacuum resistance furnace. The process is to keep the samples at 740°C for 6 hours to ensure the complete decomposition of pearlite.

The metallographic samples were made by cutting samples after heat treatment and the samples were corroded with 4% nitric acid alcohol solution. The metallographic structure and micro-shrinkage porosity were observed by Axiovert200MAT metallographic microscope and MLA250 (FEIQuanta) scanning electron microscope.

50 micro-shrinkage porosities were randomly selected in the center and edge of the samples. The maximum length and area of micro-shrinkage porosities were measured by Nano Measurer 1.2 and Photoshop software respectively, and the value is characterized by the average value of the measurement results.

3. Experimental Results and Analysis

3.1. Metallographic Microstructure

1) As-cast microstructure

The as-cast structure of two kinds of cast iron used in the experiment in Table 1 is shown in Figure 2. The matrix of them is pearlite and ferrite. Ferrite is distributed around graphite, and the amount of it is slightly more than pearlite. Most of the graphite is A-type graphites and a small portion is block graphite. Due to the high content of carbon and silicon, there is a large amount of graphite in the microstructure, as shown in Figure 2(a). The spheroidization rate of graphite in ductile iron is greater than 90%, as shown in Figure 2(b).

2) Normalized microstructure

The microstructure of two kinds of cast iron after normalizing is shown in Figure 3. After holding at 880°C and 920°C for 1 hour, there is still a part of ferrite in the microstructure, as shown in Figure 3(a) ~ (d). The lower the normalizing temperature is, the larger the amount of the pearlite is in the matrix is, that is shown in Table 2.

The experimental cast iron contains about 2% silicon, which plays a role in promoting carbon precipitation during Austenite cooling. During normalizing, the higher the heating temperature is, the longer the time that heating temperature decreases to the pearlite transition temperature is. And the larger the amount of carbon precipitates is during this period, the smaller the amount of the pearlite is. Therefore, the higher the heating temperature is, the smaller the amount of pearlite in the matrix after normalizing is when the silicon content in cast iron is 2%.

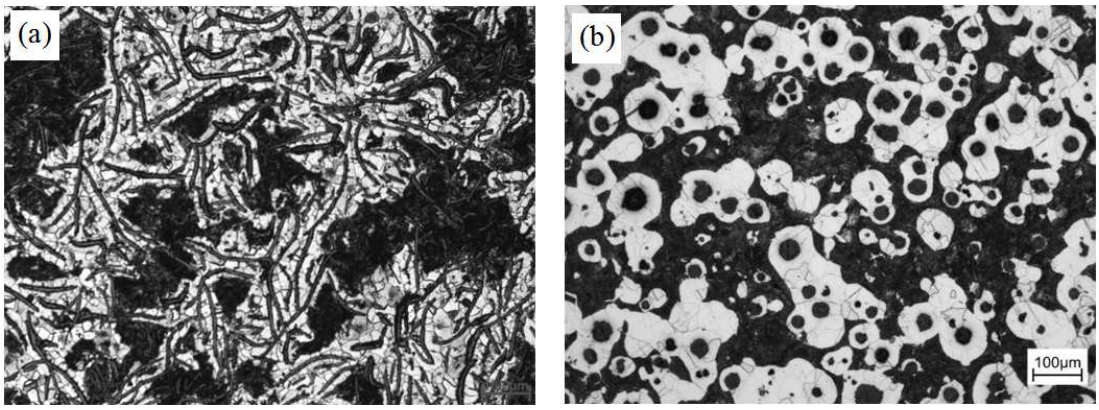

Figure 2. *As-cast structure: (a) grey cast iron; (b) ductile iron.*

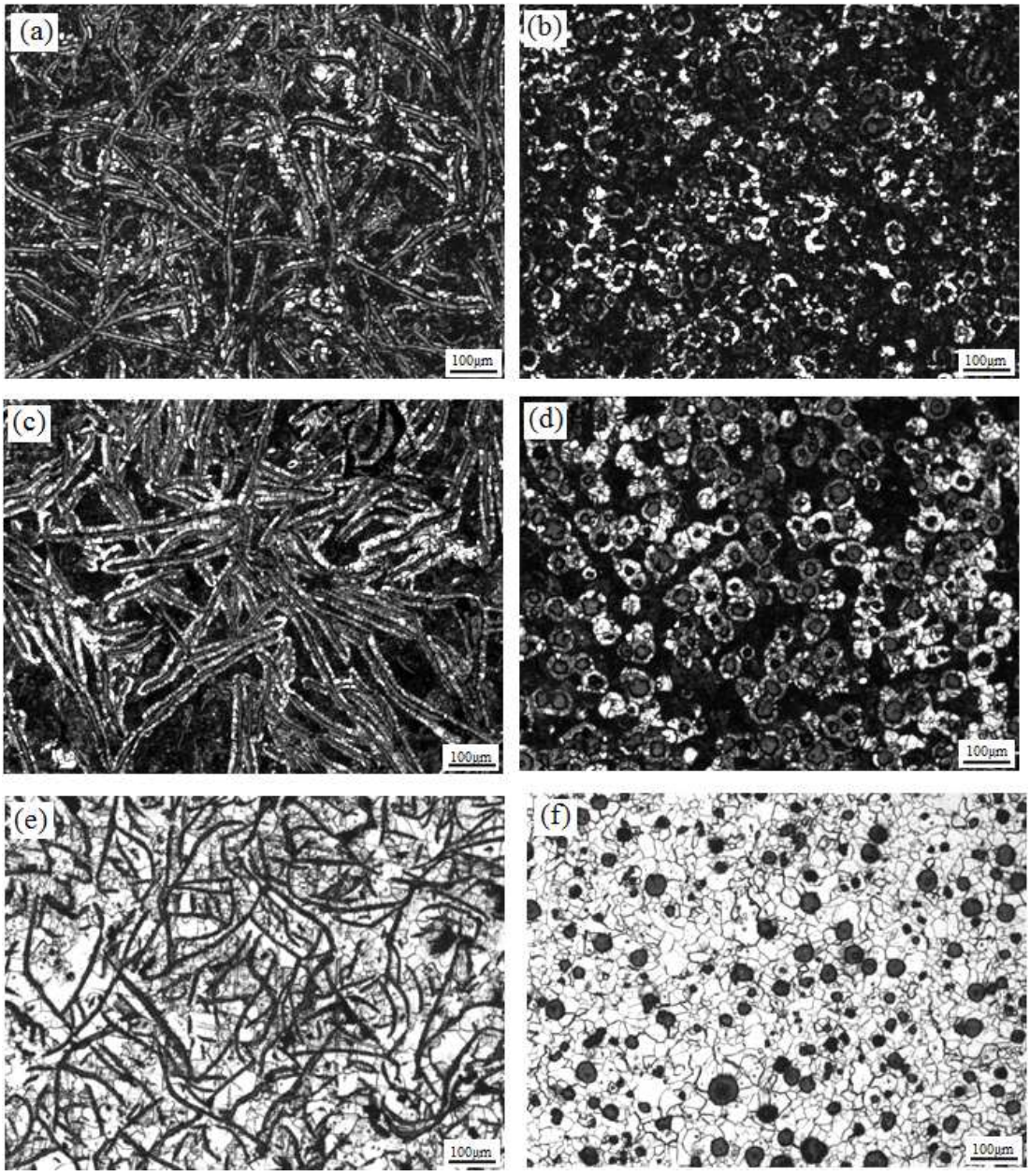

Figure 3. *Metallographic microstructures of cast iron after heat treatment: (a) (b) normalizing at 880°C; (c) (d) normalizing at 920°C; (e) (f) annealing at 740°C.*

3) Annealing microstructure after secondary graphitization

The metallographic microstructures of vacuum annealing samples after holding at 740°C for 6 hours is shown in Figure 3(e) ~ (f). After secondary graphitization annealing, all pearlite in the original matrix transformed into ferrite. It can be found that after secondary graphitization annealing, a part of point graphite appears in the microstructure by comparing Figure 3(a) ~ (f).

When pearlite in cast iron decomposes, one part of the precipitated carbon is deposited on eutectic graphite that does not affect the shape of the original graphite due to the limited amount of precipitated carbon. The other part of the precipitated carbon tramsformed into the new graphite nuclei and grow away from eutectic graphite. Due to the small amount of carbon precipitated, point graphite is formed.

3.2. Effect of Secondary Graphitization Annealing on Volume Change Rate

The results of sample size and volume change after secondary graphitization annealing are shown in Table 2. Expansion appears in the two kinds of cast iron after secondary graphitization annealing. The different expansion rate of the same cast iron is due to the different amount of pearlite in the matrix microstructure. According to the measured results of pearlite quantity in the sample, the conversion results of sample expansion rate are shown in Table 4. The results shows that the expansion rate of the samples is basically similar when the amount of pearlite in the tissue is the same.

The measured and converted results of expansion rate in Tables 2 and 4 show that the expansion rate of gray cast iron is greater than that of nodular cast iron after secondary graphitization annealing. When gray cast iron solidifies, flake graphite always grows earlier than austenite. Molten iron can get the feeding of expansion when it shrinks between eutectic groups. Therefore, it is not easy to produce micro-shrinkage porosity between eutectic groups. It is easy to form micro-shrinkage porosity between eutectic groups of nodular cast iron. The micro-shrinkage porosity in nodular cast iron counteracts part of the expansion that results in a slightly smaller expansion rate of the samples.

3.3. Effect of Secondary Graphitization Annealing on Micro-shrinkage Porosity of Ductile Iron

The scanning electron microscope photos of the metallographic sample of ductile iron are shown in Figure 4. It can be clearly seen that there is micro-shrinkage porosity on the ferrite matrix in the pictures that is shown by the arrow in Figure 4. It can be clearly seen that the sharp corner of this micro-shrinkage porosity is very sharp, and the radius of curvature of its tip is close to zero.

The measurement results of the maximum length and area of micro-shrinkage porosity are shown in Table 3. The distribution of measurement results of the length and area of 50 micro-shrinkage porosities is shown in Figure 5. Although the size distribution of micro-shrinkage porosity is disperse and the deviation of it is large, the number of micro-shrinkage porosity with large-size is small, so the average value the size can reflect the trend of micro-shrinkage porosity size.

The length and area of micro-shrinkage porosity decreased after the secondary graphitization annealing of nodular cast iron. It was found that the change of micro-shrinkage porosity in the core of the sample was more obvious. The results show the secondary graphitization annealing is critical to reduce the micro-shrinkage porosity of ductile iron.

Table 2. *Measurement results of sample size change before and after secondary graphitization.*

Heat treatment process	State	Grey cast iron				Ductile iron			
		Sample size (mm)	Volume V_{HT} (mm^3)	Expansion rate δ_{HT} (%)	Pearlite w_{HT} (%)	Sample size (mm)	Volume V_{QT} (mm^3)	Expansion rate δ_{QT} (%)	Pearlite w_{QT} (%)
Normalizing at 880°C annealing at 740°C	normalizing	a $50.12^{+0.08}_{-0.12}$	11142.1	1.41	94.9	$50.14^{+0.06}_{-0.04}$	19806.0	1.11	89.4
		b $14.90^{+0.02}_{-0.02}$				$19.91^{+0.01}_{-0.01}$			
		c $14.92^{+0.02}_{-0.02}$				$19.84^{+0.02}_{-0.04}$			
	annealing	a $5.032^{+0.06}_{-0.02}$	11269.2			$50.19^{+0.11}_{-0.05}$	20025.8		
		b $14.95^{+0.03}_{-0.05}$				$20.01^{+0.09}_{-0.07}$			
		c $14.98^{+0.04}_{-0.06}$				$19.94^{+0.12}_{-0.06}$			
normalizing at 920°C annealing at 740°C	normalizing	a $40.24^{+0.07}_{-0.04}$	8654.1	1.00	68.9	$50.35^{+0.07}_{-0.05}$	19411.6	0.81	72.6
		b $14.67^{+0.09}_{-0.05}$				$19.63^{+0.01}_{-0.03}$			
		c $14.66^{+0.04}_{-0.04}$				$19.64^{+0.02}_{-0.02}$			
	annealing	a $40.34^{+0.06}_{-0.04}$	8740.8			$50.37^{+0.08}_{-0.1}$	19567.9		
		b $14.71^{+0.03}_{-0.03}$				$19.71^{+0.02}_{-0.06}$			
		c $14.73^{+0.03}_{-0.01}$				$19.71^{+0.02}_{-0.02}$			

Note: HT represents gray cast iron and QT represents ductile iron in the table.

Table 3. *Measurement results of maximum length and area of micro-shrinkage porosity.*

cast state	**micro-shrinkage porosity size λ_{max} (μm)**		**micro-shrinkage porosity area S (μm^2)**	
	$3.84^{+2.95}_{-1.57}$		$87.27^{+244.6}_{-80.0}$	
annealed state	Sample center	Sample edge	Sample center	Sample edge
	$2.37^{+1.63}_{-1.15}$	$3.48^{+1.33}_{-1.28}$	$59.65^{+127.5}_{-49.2}$	$80.75^{+266.7}_{-72.1}$
reduction rate (%)	38.3	9.4	31.7	7.5

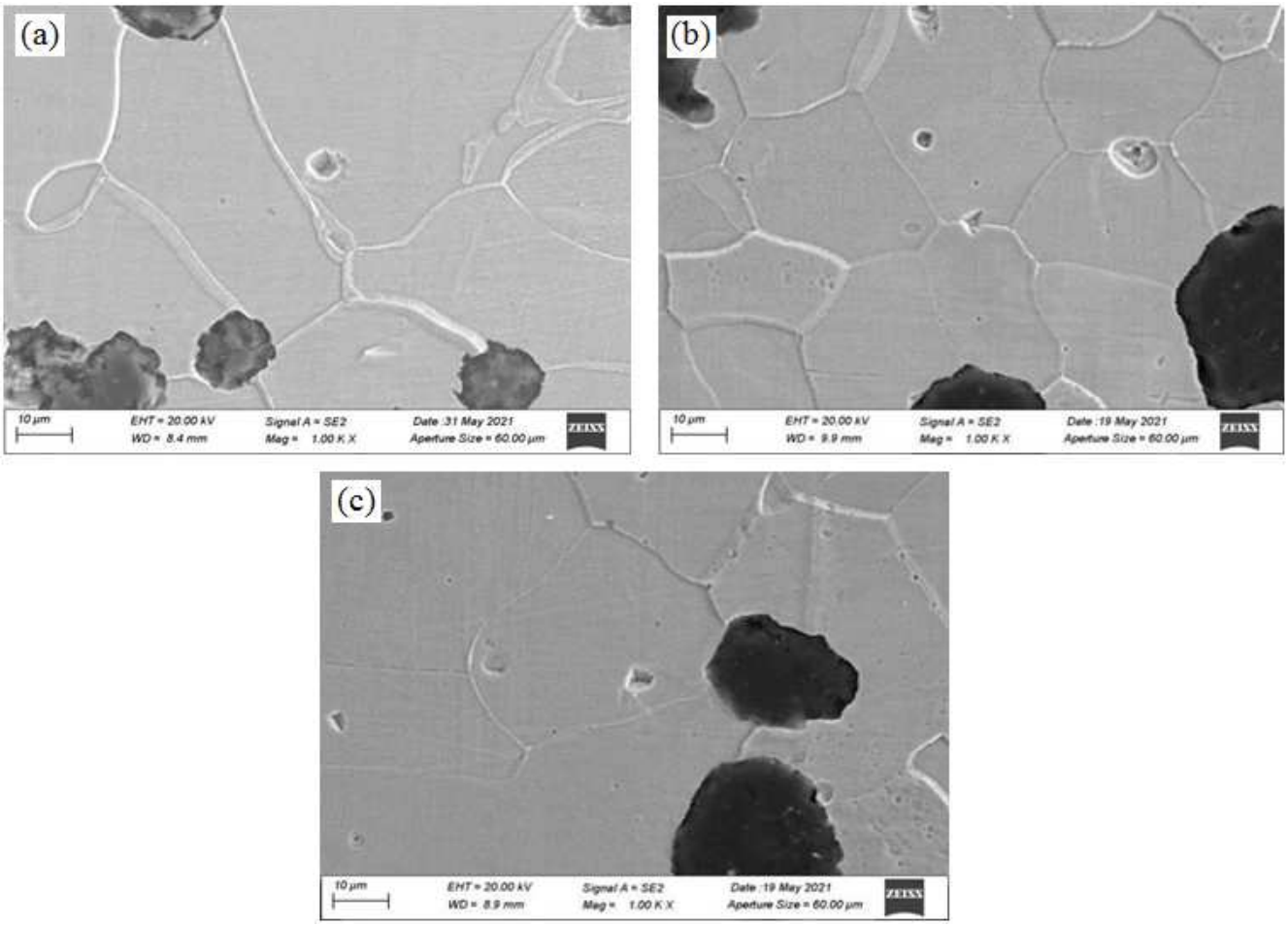

Figure 4. *Micro-shrinkage porosity in ductile iron: (a) cast iron; (b) annealed state, the core of the sample; (c) annealed state, and edge of the sample.*

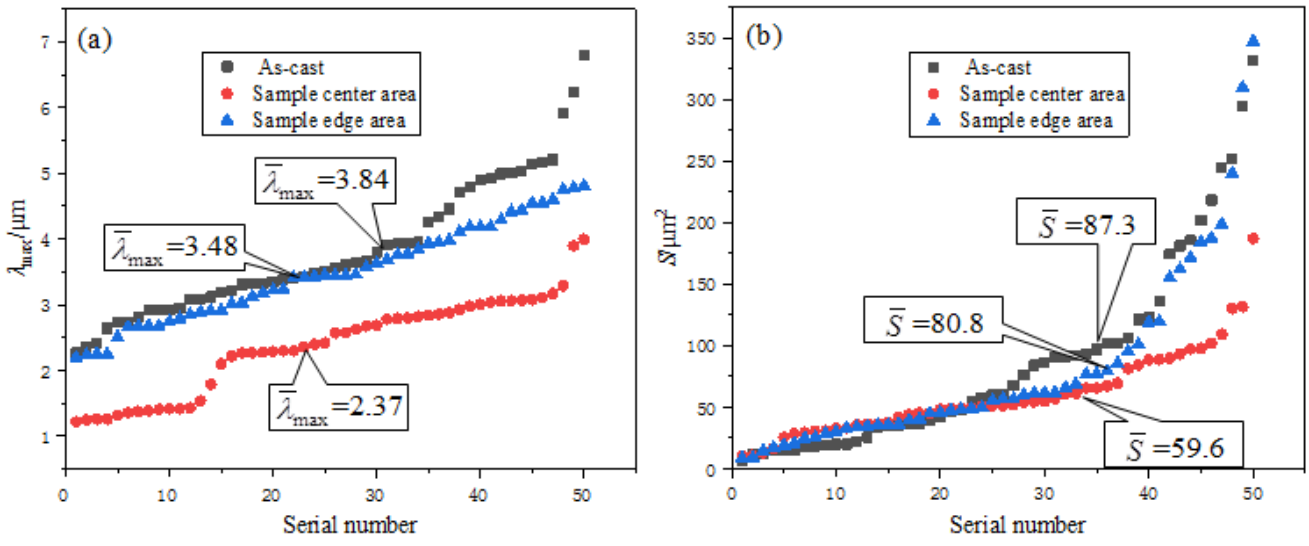

Figure 5. *Length and area of distribution of micro-shrinkage porosity: (a) length; (b) area.*

4. Discussion

4.1. Estimation of Volume Change After Pearlite Decomposition

4.1.1. Volume Change Caused by Graphite Precipitation

When the silicon content in cast iron is 2.0%, about 0.65% of carbon changes into graphite after pearlite is transformed into ferrite. Pearlite density is 7.8g.cm^{-3}, graphite cell is a = 0.1421nm, c = 0.6708nm, as shown in Figure 6. It can be estimated that the volume expansion rate due to graphite precipitation is about 1.49%.

4.1.2. Volume Change Caused by the Transformation of Cementite into Ferrite

There are four triangular prisms in the cementite cell that are shown in Figure 7(a). Two iron atoms of the cementite cell belong to two triangular prisms, so there are three iron atoms and one carbon atom in the triangular prism. The four triangular prisms are arranged in a double-layer, reverse and staggered manner across adjacent cells [20].

The shape and size of the triangular prism shown in Figure 7(a) are very close to which of the $A_0B_0D_0E_0F_0G_0$ triangular prism in Figure 7(b). Once the carbon atoms in the triangular prism shown in Figure 7(a) leave, it is easiest to form the triangular prism shown in Figure 7(b). After a cementite triangular prism is transformed into a ferrite triangular prism, the volume expansion rate is 4.09%.

The arrangement of four triangular prisms across adjacent crystal cells will enlarge the spacing of iron atoms adjacent to the triangular prism. According to the specific size of the triangular prism shown in Figure 7(a), it can be estimated that it is enlarged by 0.011nm, 0.017nm and 0.098nm in three directions respectively. When the iron atoms in this part return to ferrite, the volume shrinkage is about 2.92%.

In conclusion, the volume expansion rate after the transformation of cementite into ferrite is about 1.17%.

4.1.3. Volume Expansion Rate After Pearlite Decomposition

Cementite in pearlite accounts for 12%, so the volume expansion rate caused by cementite decomposition is 0.141%. The volume expansion rate caused by cementite decomposition is about 1.63%.

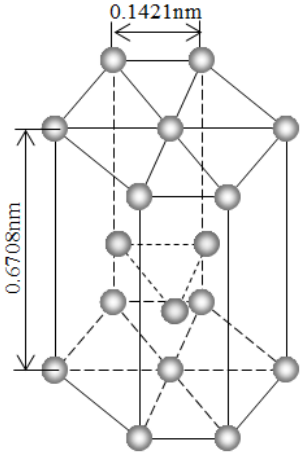

Figure 6. *Schematic diagram of graphite cell.*

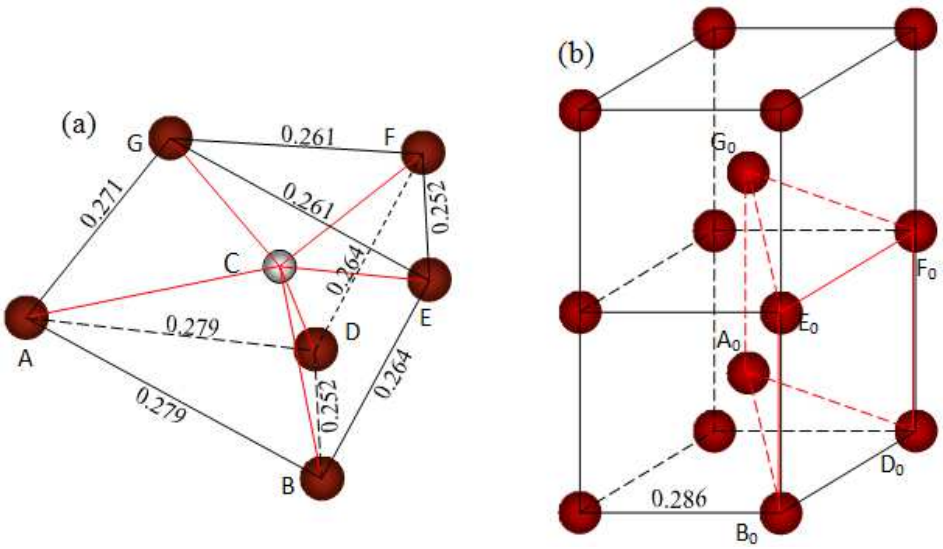

Figure 7. *Crystal structures of cementite and α_{Fe}: (a) triangular prism in cementite cell; (b) Triangular prism in α_{Fe} crystal cell.*

According to the quantity of pearlite in the matrix microstructure of nodular cast iron and the test results of sample expansion rate, the expansion rate produced by pearlite decomposition can be converted that is shown in Table 4. It can be determined from the results that the theoretical estimation is basically consistent with the experimental results that is shown in Table 4.

The following reasons lead to the difference between theoretical estimation and experimental results. First, the assumption that the triangular prism in cementite cell changes into the triangular prism in ferrite and the triangular prism in cementite that causes the change of the spacing of surrounding iron atoms is different from the actual crystal structure of cementite. Second, the micro-shrinkage porosity in the sample

will consume part of the expansion.

4.2. The Process of Reducing Micro Porosity by Secondary Graphitization Expansion

According to the variation law of yield strength of Fe-0.06C-1.5Mn-13Cr ferritic stainless steel with temperature given by Lou [21], when the temperature is 740°C, the yield strength is about 30MPa. It is estimated that the yield strength of pure ferrite is less than 10MPa at 740°C without strengthening effect of Cr. Therefore, it can be determined that the ferrite of nodular cast iron matrix is easy to deform at 740°C.

Table 4. *Volume expansion rate after secondary graphitization.*

Cast iron type	Pearlite quantity (%)	Experimental expansion rate (%)		Estimated Expansion Rate (%)
		Samples	pearlite	
Grey cast iron	94.9	1.41	1.49	1.63
	68.9	1.00	1.45	
Ductile iron	89.4	1.11	1.24	
	72.6	0.81	1.12	

An austenitic shell is formed around the graphite ball due to the lack of carbon in the molten iron around the graphite ball when nodular cast iron solidifies and the graphite ball grows to a certain extent. At the later stage of solidification, the molten iron between spherical austenite is not supplemented by molten iron during solidification, resulting in micro-shrinkage porosity, as shown in Figure 8(a).

The expansion force generated by secondary graphitization of nodular cast iron forces the ferrite to undergo plastic deformation. Because there is no barrier in the micro-shrinkage porosity, the ferrite can fill micro-shrinkage porosity. If the micro-shrinkage porosity formed during solidification is small, the secondary graphitization expansion can completely eliminate it. For the micro-shrinkage porosity with larger size, the secondary graphitization expansion can also reduce it, as shown in Figure 8(b) ~ (c).

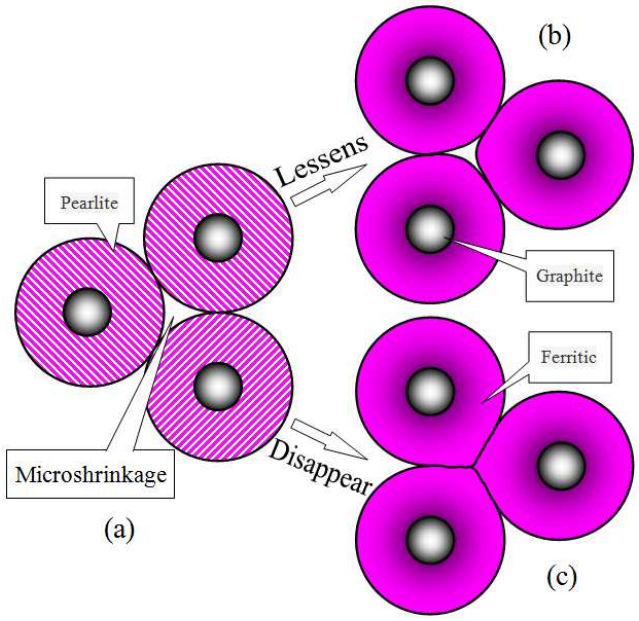

Figure 8. *Schematic diagram of process of filling micro-shrinkage porosity by ferrite.*

During secondary graphitization annealing, it is not easy for the ferrite near the edge of the sample to fill micro-shrinkage porosity during deformation that results in a small change in the size of micro-shrinkage porosity in the edge of the sample because the sample is not constrained by the outside world. It is easy for the ferrite fill micro-shrinkage porosity during deformation which significantly reduces the size of micro-shrinkage porosity in this area taht is shown in Table 3 because the core area of the sample is subject to its own constraints.

If the reduction in size and quantity of micro-shrinkage porosity after casting is defined as the self-repair ability of micro-shrinkage porosity of ferrite ductile iron, the greater the secondary graphitization expansion is, the stronger the self-repair ability is. So it is significant to obtain pearlite ductile iron before secondary graphitization annealing.

Strengthening inoculation treatment and fining graphite balls are not only good for reducing the micro-shrinkage porosity formed during solidification of ductile iron, but also good for improving the self-repair ability of micro-shrinkage porosity of ferrite ductile iron.

5. Conclusions

The secondary graphitization annealing leads to the expansion of cast iron. The larger the amount of pearlite is, the greater the expansion is. The volume expansion rates of ductile iron and gray cast iron after secondary graphitization annealing are about 1.2% and 1.4% respectively.

After secondary graphitization annealing, the size and quantity of micro-shrinkage porosity of ductile iron decrease. That is to say, the ferrite ductile iron has the ability to repaire micro-shrinkage porosity.

The theoretical estimation results of expansion rate after secondary graphitization of cast iron are basically consistent with the experimental results. The research will provide a theoretical basis for the production of ferritic ductile iron with high toughness in the ultra-low temperature.

Acknowledgements

The authors acknowledge the financial support provided by Major Science and Technology Project of Liaoning Province, China (No.: 1585015895240).

References

[1] Toktas G, Toktas A, Tayanc M. Influence of matrix structure on the fatigue properties of an alloyed ductile iron. Materials and Design, 2008, 29 (8): 1600-1608.

[2] Zhang K, Liu J D, Song X F, et al. Investigation on low-temperature impact toughness of heavy-section nodular iron. Modern Cast Iron, 2017, 37 (3): 41-45.

[3] David P, Massone J, Boeri R, et al. Mechanical properties of thin wall ductile iron-influence of carbon equivalent and graphite distribution. ISIJ International, 2004, 44 (7): 1180-1187.

[4] Caldera M, Massone J M, Boeri R E, et al. Impact properties of thin wall ductile iron. ISIJ International, 2004, 44 (4): 731-736.

[5] Torsten S G, Ingvar L S. The effect of graphite fraction and morphologyon the plastic deformation behavior of cast irons. Metallurgical andMaterialsTransactionsA, 2007, 38 (4): 840-847.

[6] Iacoviello F, Cocco V D. Influence of the graphite elements morphology on the fatigue crack propagation mechanisms in a ferritic ductile cast iron. Engineering Fracture Mechanics, 2016, 167 (11): 248-258.

[7] Costa Nuno, Machado Nuno, Silva Filipe Samuel. Influence of graphite nodules geometrical featureson fatigue life ofhigh-strength nodularcastiron. JMEPEG, 2008, 17 (3): 352-362.

[8] Chen D, Sang w w, Wu L X, et al. Study on Thermal Fatigue Crack Initiation and Propagation Behavior in Nodular Cast Iron. Foundry Technology, 2018, 39 (2): 482-432.

[9] Diao X G, Ning Z L, Cao F Y, et al. Graphite morphology evolution during melt holding of ductile iron. Key Engineering Materials, 2011, 457: 31-36.

[10] Herbert Werner. Mischkristallverfestigte EN-GJS-Werkstoff fuer Gross-und Schwergussteile. Giesserei, 2016, 103 (2): 38-42.

[11] Jacaze J, Larranaga P, Asenjo I, et al. Sertucha Influence of 1wt% addijion of Ni on structural and mechanical properties of ferritic ductile irons. Materials Science and Technology, 2012, 28 (5): 603-608.

[12] Sun Y F, Hu S M, Xiao Z Y, et al. Effects of nickel on low-temperature impact toughness and corrosion resistance of high-ductile iron. Materials and Design, 2012, 41: 37-42.

[13] Zhang X N, Qu Y D, Yang H W, et al. Temperature impact toughness and fracture mechanism of cast QT400-18L ductile iron with different Ni additions. China Foundry, 2013, 10 (5): 310-314.

[14] Chen X G, Xu J, Hu H, et al. Effects of niobium addition on microstructure and tensile behavior of as-cast ductile iron. Materials Science and Engineering A, 2017, 688 (3): 416-428.

[15] Verdu C, Adrien J, Buffière J Y. Three-dimensional shape of the early stages of fatigue cracks nucleated in nodular cast iron. Materials science and engineering A, 2008, 483-484: 402-405.

[16] Verdu C, Adrien J, Reynaud A. Contributions of dual phase heat treatments to fatigue properties of SG cast irons. International Journal of Cast Metal Research, 2005, 18 (6): 346-354.

[17] Guo E J. Effect of Ce-Mg-Si and Y-Mg-Si nodulizers on the microstructures and mechanical properties of heavy section ductile iron. Journal of rare earths, 2014. 32 (8): 38-744.

[18] Gao M Q, Li G L, You J H. Cementites decomposition of a pearlitic ductile cast iron during graphitization annealing heat treatment. Journal of iron and steel research international. 2017. 24: 838-843.

[19] Hou Chao, Rrn Wei, Song Jia-jian, et al. Effects of Microshrinkage on Low Temperature Toughness of Ferritic Ductile Iron. Fundry, 2019, 68 (2): 123-127.

[20] Cai Hong, Lu Jun, Wang Zhi-ming, et al. Structure of Cementite and Morphology of Primary Cementite. Heat Treatment, 2010, 25 (2): 50-53.

[21] Lou Guobiao, Tao Yuchao, Chen Wulong, et al. Experimental Investigation of Mechanical Properties of TSZ410 Ferritic Stainless Steel at Elevated Temperature. JOURNAL OF TONGJI UNIVERSITY (NATURAL SCIENCE), 2021, 49 (1): 20-29.